Quantum walk search on Kronecker graphs

Thomas G. Wong,[1,*] Konstantin Wünscher,[2,†] Joshua Lockhart,[3,‡] and Simone Severini[3,4,§]

[1]*Department of Physics, Creighton University, 2500 California Plaza, Omaha, Nebraska 68178, USA*
[2]*Department of Statistical Science, University College London, 1-19 Torrington Place, London WC1E 7HB, United Kingdom*
[3]*Department of Computer Science, University College London, Gower Street, London WC1E 6BT, United Kingdom*
[4]*Institute of Natural Sciences, Shanghai Jiao Tong University, Shanghai 200240, China*

Kronecker graphs, obtained by repeatedly performing the Kronecker product of the adjacency matrix of an "initiator" graph with itself, have risen in popularity in network science due to their ability to generate complex networks with real-world properties. We explore spatial search by continuous-time quantum walk on Kronecker graphs. Specifically, we give analytical proofs for quantum search on first-, second-, and third-order Kronecker graphs with the complete graph as the initiator, showing that search takes Grover's $O(\sqrt{N})$ time. Numerical simulations indicate that higher-order Kronecker graphs with the complete initiator also support optimal quantum search.

I. INTRODUCTION

Grover's algorithm [1] is a foundational algorithm in quantum computing [2] that searches an unordered database of N items in $O(\sqrt{N})$ time, thus offering a quadratic speedup over classical search. However, Benioff [3] notes that the runtime can be slower when searching a spatial region, since the time taken for a quantum robot or cellular automata [4,5] to traverse the physical database must be taken into consideration. Since then, much research has explored how quickly quantum computers search various spatial regions. See [6–8] for some seminal papers, and [9–11] for some recent results. The structure of the physical database can be encoded as a combinatorial graph, the goal being to find a particular "marked" vertex using the least possible number of queries to an oracle encoding the graph structure. Often, the quantum search is performed using a quantum walk [12], which respects the locality of the graph.

Most of the graphs on which quantum search has been analyzed have translational symmetry or some other structure that makes the behavior of the quantum algorithm amenable to rigorous proof. These constraints mean that the graphs considered are often very different from real-world networked data (henceforth, "networks"), which are typically *small world* [13], meaning the number of edges between any pair of nodes is small. The degree distributions of real-world networks are often scale free, heavy tailed, or follow power laws [14]. The question of how quantum walk search performs on real-world networks has received much less attention.

To attack this question, one might consider investigating the behavior of quantum search on real-world networked datasets (see, for example, the Stanford Large Network Dataset

Collection [15]). However, we are mostly interested in how the runtime of the search algorithm depends on the number of nodes N, and since these datasets are typically static with a fixed number of nodes, they are not suitable for this purpose. To determine the dependence on N, one would need to extrapolate the network to the future or rewind a network to the past, which is made difficult by the fact that randomly removing vertices destroys the degree distribution of the network [16].

One solution to this is to use Kronecker graphs [17–20] to generate synthetic networks that have some or all of the aforementioned real-world properties. Kronecker graphs can be "grown" iteratively, to include as many vertices as desired, and so they are suitable for our purposes. To produce a Kronecker graph, one begins with an "initiator" graph of M vertices and its associated adjacency matrix A, where $A_{uv} = 1$ if vertices u and v are adjacent, and 0 otherwise. The jth-order Kronecker graph is the graph whose adjacency matrix is $A^{\otimes j}$, the Kronecker or tensor product of A with itself j times, i.e.,

$$A^{\otimes j} = \underbrace{A \otimes A \otimes \cdots \otimes A}_{j \text{ times}}.\tag{1}$$

This defines a graph with $N = M^j$ vertices. Kronecker graphs can also be made stochastic, and they have been used to accurately model the arXiv citation graph, the internet at the level of autonomous systems, citations of U.S. patents, the coauthor network, and the trust network of Epinions [20].

Besides their ability to be fitted to real-world datasets, Kronecker graphs have another advantage over other methods for generating real-world networks, such as the preferential attachment model [14]. As real-world networks grow, the number of edges they sprout is typically more than the number of nodes. This means the network gets more dense over time and the effective diameter tends to shrink. The preferential attachment model does not capture this, but Kronecker graphs do [17,18].

In this paper, we report our first steps toward understanding how quantum walks search Kronecker graphs by analyzing the case where the initiator is the complete graph, or all-to-all

*thomaswong@creighton.edu
†konstantin.wuenscher.16@ucl.ac.uk
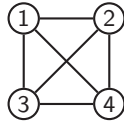‡joshualockhart@gmail.com
§s.severini@ucl.ac.uk

FIG. 1. K_4, the complete graph, or all-to-all network, of four vertices.

network. We denote the complete graph of M vertices by K_M, and the jth-order Kronecker graph generated by it by $K_M^{\otimes j} = K_M \otimes K_M \otimes \cdots \otimes K_M$. This is an ideal Kronecker graph to begin with because, as we will see subsequently, it is amenable to rigorous analysis. We give proofs that the first-, second-, and third-order Kronecker graphs with complete initiator can be searched by a continuous-time quantum walk in $\pi\sqrt{N}/2$ time, which is the optimal $O(\sqrt{N})$ runtime of Grover's algorithm [21]. A continuous-time quantum walk searches [7] by starting in a uniform superposition $|s\rangle$ over all N vertices:

$$|\psi(0)\rangle = |s\rangle = \frac{1}{\sqrt{N}} \sum_{i=1}^{N} |i\rangle, \qquad (2)$$

where $|1\rangle, |2\rangle, \ldots, |N\rangle$ are the computational basis states that label the vertices. Then the system evolves by Schrödinger's equation $i\,d\psi/dt = H\psi$ (with $\hbar = 1$) with Hamiltonian

$$H = -\gamma A^{\otimes j} - |w\rangle\langle w|, \qquad (3)$$

where γ is the jumping rate (amplitude per time) of the quantum walk, and $|w\rangle$ denotes the marked vertex we are looking for [7]. We end by showing results of numerical simulations that suggest higher-order Kronecker graphs, with the complete initiator, can also be quickly searched in the same $\pi\sqrt{N}/2$ time. For search on deterministic and stochastic Kronecker graphs with incomplete initiators that produce graphs with real-world properties, we will report our findings separately.

II. FIRST ORDER

In this section, we analyze search on the first-order Kronecker graph with complete initiator. From the definition of Kronecker graphs (1) with $j = 1$, the first-order Kronecker graph is simply the complete initiator graph itself. For example, the complete graph with four vertices is shown in Fig. 1, and
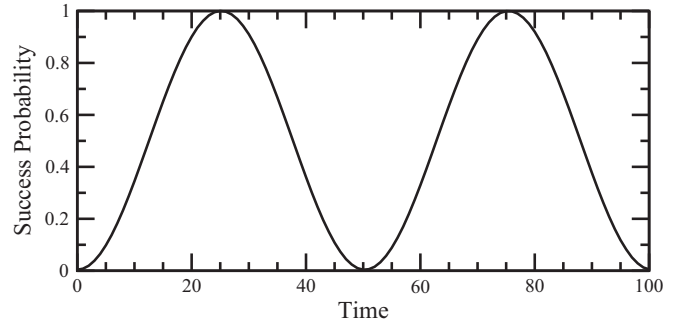

FIG. 2. Success probability as a function of time for search by continuous-time quantum walk on the complete graph K_M with $M = 256$.

its adjacency matrix is

$$A = \begin{pmatrix} 0 & 1 & 1 & 1 \\ 1 & 0 & 1 & 1 \\ 1 & 1 & 0 & 1 \\ 1 & 1 & 1 & 0 \end{pmatrix}.$$

If the initiator has M vertices, then the first-order Kronecker graph has $N = M$ vertices.

Search on the complete graph is exactly the quantum walk formulation of Grover's unstructured search algorithm since a complete graph constitutes an unstructured database. As shown in [7], when the jumping rate γ takes a "critical value" of $1/N$, the algorithm is equivalent to the "analog analogue" of Grover's algorithm [22]. Then the system evolves from the initial uniform superposition state $|s\rangle$ to the marked state $|w\rangle$ (up to a phase) in time $\pi\sqrt{N}/2 = O(\sqrt{N})$ [23]. Measuring the position of the walker at this time, one is certain to find it at the marked vertex. A simulation is shown in Fig. 2, and the success probability reaches 1 at time $\pi\sqrt{256}/2 \approx 25.13$, as expected.

III. SECOND ORDER

Next, we consider the second-order Kronecker graph with complete initiator, which is also the line graph of a complete bipartite graph [24]. For example, if the initiator is the complete graph of $M = 4$ vertices from Fig. 1, then the second-order Kronecker graph has $N = M^2 = 4^2 = 16$ vertices, and its adjacency matrix is

$$A^{\otimes 2} = A \otimes A = \begin{pmatrix} 0 & A & A & A \\ A & 0 & A & A \\ A & A & 0 & A \\ A & A & A & 0 \end{pmatrix} = \begin{pmatrix}
0 & 0 & 0 & 0 & 0 & 1 & 1 & 1 & 0 & 1 & 1 & 1 & 0 & 1 & 1 & 1 \\
0 & 0 & 0 & 0 & 1 & 0 & 1 & 1 & 1 & 0 & 1 & 1 & 1 & 0 & 1 & 1 \\
0 & 0 & 0 & 0 & 1 & 1 & 0 & 1 & 1 & 1 & 0 & 1 & 1 & 1 & 0 & 1 \\
0 & 0 & 0 & 0 & 1 & 1 & 1 & 0 & 1 & 1 & 1 & 0 & 1 & 1 & 1 & 0 \\
0 & 1 & 1 & 1 & 0 & 0 & 0 & 0 & 0 & 1 & 1 & 1 & 0 & 1 & 1 & 1 \\
1 & 0 & 1 & 1 & 0 & 0 & 0 & 0 & 1 & 0 & 1 & 1 & 1 & 0 & 1 & 1 \\
1 & 1 & 0 & 1 & 0 & 0 & 0 & 0 & 1 & 1 & 0 & 1 & 1 & 1 & 0 & 1 \\
1 & 1 & 1 & 0 & 0 & 0 & 0 & 0 & 1 & 1 & 1 & 0 & 1 & 1 & 1 & 0 \\
0 & 1 & 1 & 1 & 0 & 1 & 1 & 1 & 0 & 0 & 0 & 0 & 0 & 1 & 1 & 1 \\
1 & 0 & 1 & 1 & 1 & 0 & 1 & 1 & 0 & 0 & 0 & 0 & 1 & 0 & 1 & 1 \\
1 & 1 & 0 & 1 & 1 & 1 & 0 & 1 & 0 & 0 & 0 & 0 & 1 & 1 & 0 & 1 \\
1 & 1 & 1 & 0 & 1 & 1 & 1 & 0 & 0 & 0 & 0 & 0 & 1 & 1 & 1 & 0 \\
0 & 1 & 1 & 1 & 0 & 1 & 1 & 1 & 0 & 1 & 1 & 1 & 0 & 0 & 0 & 0 \\
1 & 0 & 1 & 1 & 1 & 0 & 1 & 1 & 1 & 0 & 1 & 1 & 0 & 0 & 0 & 0 \\
1 & 1 & 0 & 1 & 1 & 1 & 0 & 1 & 1 & 1 & 0 & 1 & 0 & 0 & 0 & 0 \\
1 & 1 & 1 & 0 & 1 & 1 & 1 & 0 & 1 & 1 & 1 & 0 & 0 & 0 & 0 & 0
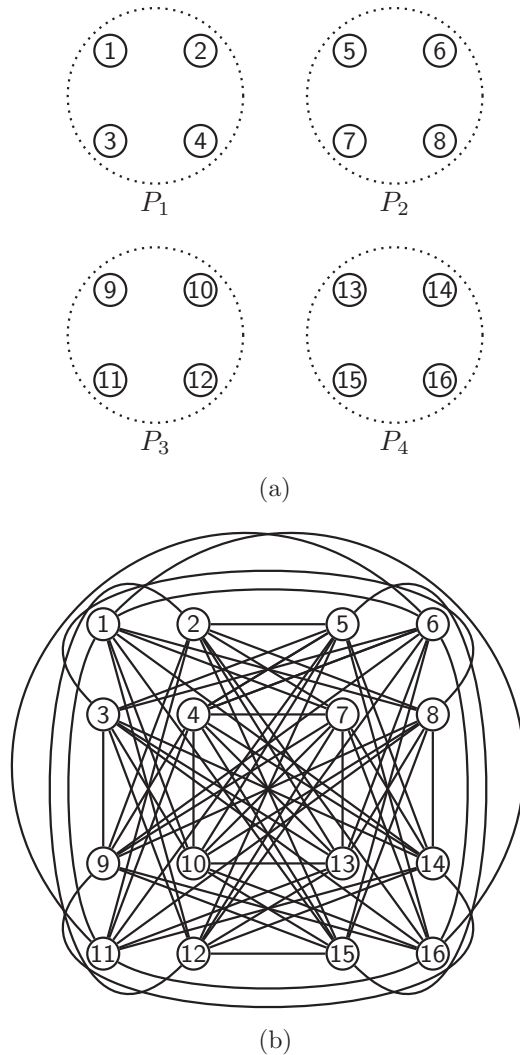\end{pmatrix}.$$

(a)

(b)

FIG. 3. (a) Four sets of four vertices. (b) The second-order Kronecker graph $K_4 \otimes K_4$.

To draw this Kronecker graph, we begin with the initiator K_4 in Fig. 1 and replace each vertex with four new nodes, as shown in Fig. 3(a), grouping them in sets P_1 through P_4. Now, consider a specific vertex, say vertex 1. First, it is not connected to any other vertices in its set P_1. Next, note vertex 1 is in the top-left corner of P_1 and, similarly, vertex 5 is in the top-left corner of P_2, vertex 9 is in the top-left corner of P_3, and vertex 13 is in the top-left corner of P_4. Vertex 1 is adjacent to all vertices in the other partite sets except these that share the same top-left position. So vertex 1 is adjacent to vertices 6, 7, and 8 in P_2, vertices 10, 11, and 12 in P_3, and vertices 14, 15, and 16 in P_4. Following this procedure for each vertex, the Kronecker graph $K_4 \otimes K_4$ is shown in Fig. 3(b). Note that P_1, P_2, P_3, and P_4 are partite sets of a four-partite graph.

To determine how quickly a continuous-time quantum walk searches second-order Kronecker graphs with the complete initiator, we next prove that $K_M \otimes K_M$ is a strongly regular graph [25]. A strongly regular graph (N, k, λ, μ) is a graph of N vertices where every vertex has k neighbors, adjacent vertices share λ common neighbors, and nonadjacent vertices share μ common neighbors. How quickly a continuous-time
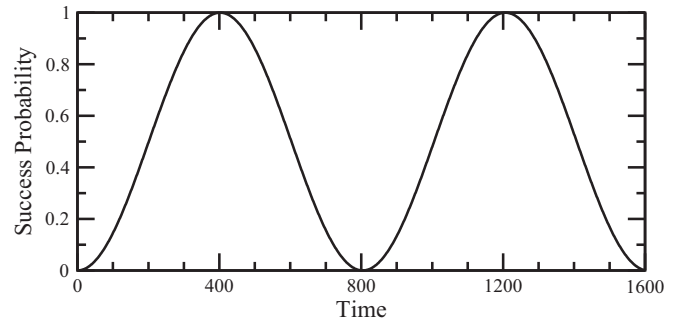

FIG. 4. Success probability as a function of time for search by continuous-time quantum walk on $K_M \otimes K_M$ with $M = 256$.

quantum walk searches a strongly regular graph, depending on its parameters, was investigated in [9].

To determine the parameters of the strongly regular graph, let us work through the example of $K_4 \otimes K_4$ in Fig. 3(b). Then, we will generalize it to arbitrary $K_M \otimes K_M$. First, every vertex is adjacent to three vertices in three partite sets, so the graph is regular with degree $3^2 = 9$. Second, adjacent vertices must be in different partite sets, and their positions (top-left, top-right, etc.) within their partite sets must also differ. For example, vertices 1 and 6 are adjacent. There are $4 - 2 = 2$ remaining partite sets in which they have mutual neighbors, and each of these partite sets has $4 - 2 = 2$ positions within them containing mutual neighbors. So adjacent vertices have $2^2 = 4$ mutual neighbors. Finally, nonadjacent vertices could be in the same partite set or in different partite sets. If the nonadjacent vertices are in the same partite set, such as vertices 1 and 2, then there are $4 - 1 = 3$ other partite sets that each contain $4 - 2 = 2$ mutual neighbors, for a total of $3 \times 2 = 6$ mutual neighbors. If they are in different partite sets, such as vertices 1 and 5, then they must occupy the same position within their respective sets, such as the top-left corner. This leaves $4 - 2 = 2$ other partite sets that each contain $4 - 1 = 3$ mutual neighbors, for a total of $2 \times 3 = 6$ mutual neighbors. So the number of mutual neighbors of nonadjacent vertices is the same in both cases. Combining these results, $K_4 \otimes K_4$ is strongly regular with parameters $(N, k, \lambda, \mu) = (16, 9, 4, 6)$.

Generalizing this, $K_M \otimes K_M$ is an M-partite graph that is strongly regular with parameters (N, k, λ, μ), where

$$
\begin{aligned}
N &= M^2, \\
k &= (M-1)^2, \\
\lambda &= (M-2)^2, \\
\mu &= (M-1)(M-2).
\end{aligned}
$$

From [9], if the parameters of a strongly regular graph satisfy $k = o(N)$ and $k = o[(\mu N)^{2/3}]$, then when the jumping rate γ takes a "critical value" of $1/k + 1/[(N-1)\mu]$, the continuous-time quantum walk searches the graph with probability 1 at time $\pi \sqrt{N}/2$, asymptotically. With the parameters that we derived for $K_M \otimes K_M$, k scales as $\sqrt{N}$, and $(\mu N)^{2/3}$ scales as $N^{4/3}$. So both conditions that $k = o(N)$ and $k = o[(\mu N)^{2/3}]$ are satisfied, and a continuous-time quantum walk searches the second-order Kronecker graph with complete initiator in $\pi \sqrt{N}/2$ time. A simulation is shown in Fig. 4, and
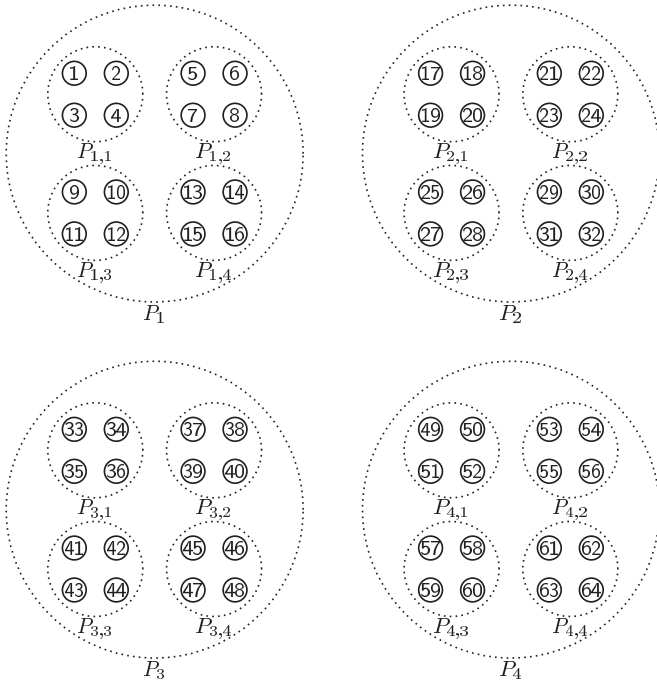
FIG. 5. The vertices of $K_4 \otimes K_4 \otimes K_4$, arranged in four sets P_i with $i = 1, 2, 3, 4$, each with four subsets $P_{i,j}$ with $j = 1, 2, 3, 4$.

the success probability reaches 1 at time $\pi\sqrt{256^2}/2 \approx 402.12$, as expected.

IV. THIRD ORDER

Now, we consider the third-order Kronecker graph. For example, using K_4 from Fig. 1 as the initiator, the third-order Kronecker graph has $N = M^3 = 4^3 = 64$ vertices, and its adjacency matrix is

$$A^{\otimes 3} = A \otimes A \otimes A$$
$$= \begin{pmatrix} 0 & A^{\otimes 2} & A^{\otimes 2} & A^{\otimes 2} \\ A^{\otimes 2} & 0 & A^{\otimes 2} & A^{\otimes 2} \\ A^{\otimes 2} & A^{\otimes 2} & 0 & A^{\otimes 2} \\ A^{\otimes 2} & A^{\otimes 2} & A^{\otimes 2} & 0 \end{pmatrix}.$$

To draw this Kronecker graph, we again begin with the initiator K_4 from Fig. 1 and replace each vertex with the 16 vertices of $K_4 \otimes K_4$ from Fig. 3(a). The result of this substitution is shown in Fig. 5, without any edges. In this figure, we grouped together sets P_i of 16 vertices, and further grouped subsets $P_{i,j}$ of four vertices.

To determine the edges, consider a specific vertex, say vertex 1, which is in the top-left corner of its subset $P_{1,1}$. Then, vertex 1 is nonadjacent to any vertex in the top-left position of its subset, so it is nonadjacent to vertices 5, 9, 13, 17, 21, 25, 29, 33, 37, 41, 45, 49, 53, 57, and 61. Vertex 1 is in subset $P_{1,1}$, which is the top-left subset within the set P_1. Then, vertex 1 is nonadjacent to the subsets $P_{1,1}$, $P_{2,1}$, $P_{3,1}$, and $P_{4,1}$, since those are the top-left subsets of their partite sets. Finally, vertex 1 is within set P_1, so it is not adjacent to any other vertex in P_1. Vertex 1 is adjacent to everything else. Explicitly drawing all the edges is messy, so we do not do so. In Fig. 6, however, the vertices adjacent to vertex 1 are colored blue.
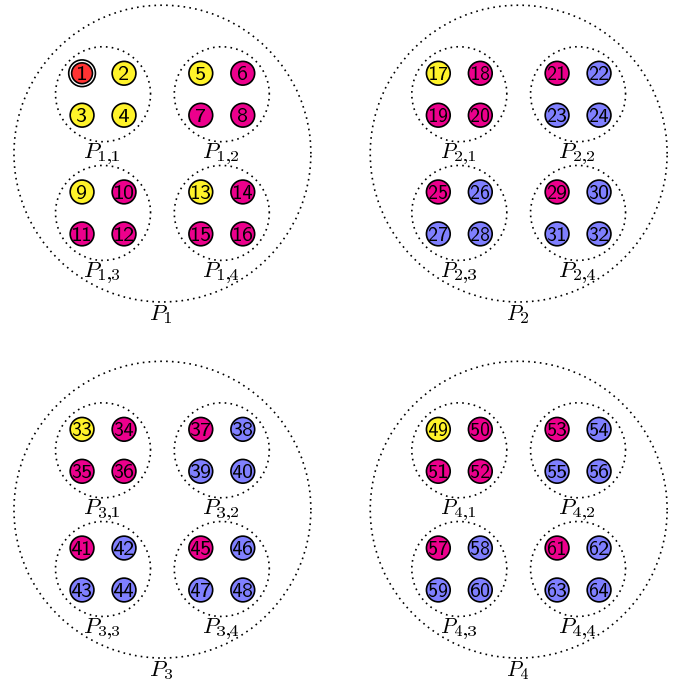

FIG. 6. The vertices of $K_4 \otimes K_4 \otimes K_4$, arranged in four sets P_i with $i = 1, 2, 3, 4$, each with four subsets $P_{i,j}$ with $j = 1, 2, 3, 4$. Vertex 1 is colored red, and identified by a double circle. Its neighbors are colored blue, and its nonadjacent vertices are colored yellow and magenta, depending on their mutual neighbors. Identically colored vertices evolve identically.

Now, note the system evolves in a four-dimensional (4D) subspace, in contrast to the first-order Kronecker graph (complete graph) that evolves in a 2D subspace [7] and the second-order Kronecker graph (strongly regular graph) that evolves in a 3D subspace [9]. This is because vertices can evolve identically to each other due to the symmetry of the graph and quantum walk. In this case, there are four types of vertices. The details are given in the Appendix, but we briefly describe them here. The first type of vertex is the marked vertex, which evolves uniquely. The second type is the vertices adjacent to the marked vertex. They evolve identically to each other, and there are $(M - 1)^3$ of them. The graph has diameter 2, so vertices nonadjacent to the marked vertex constitute the third and fourth types of vertices. Specifically, $3(M - 1)$ of these vertices share $(M - 1)^2(M - 2)$ common neighbors with the marked vertex, and $3(M - 1)^2$ of them share $(M - 1)(M - 2)^2$ mutual neighbors with the marked vertex. Altogether, there are $1 + (M - 1)^3 + 3(M - 1) + 3(M - 1)^2 = M^3 = N$ vertices, as expected. Each vertex is color coded by type in Fig. 6, with the marked vertex red, its adjacent vertices blue, and the two types of nonadjacent vertices yellow and magenta. Since the graph is vertex transitive, without loss of generality, vertex 1 can be considered to be the marked vertex.

Grouping together identically evolving vertices, the 4D subspace is spanned by

$$|a\rangle = |\text{Type 1}\rangle = |w\rangle,$$

$$|b\rangle = \frac{1}{\sqrt{(M - 1)^3}} \sum_{x \in \text{Type 2}} |x\rangle,$$

$$|c\rangle = \frac{1}{\sqrt{3(M-1)}} \sum_{x \in \text{Type } 3} |x\rangle,$$

$$|d\rangle = \frac{1}{\sqrt{3(M-1)^2}} \sum_{x \in \text{Type } 4} |x\rangle.$$

So $|a\rangle$ is the marked vertex, $|b\rangle$ are the vertices adjacent to the marked vertex, and $|c\rangle$ and $|d\rangle$ are the two types of vertices nonadjacent to the marked vertex. In this $\{|a\rangle, |b\rangle, |c\rangle, |d\rangle\}$ basis, the initial uniform superposition state (2) is

$$|s\rangle = \frac{1}{\sqrt{N}} \begin{pmatrix} 1 \\ \sqrt{(M-1)^3} \\ \sqrt{3(M-1)} \\ \sqrt{3(M-1)^2} \end{pmatrix},$$

and the adjacency matrix is

$$A^{\otimes 3} = \begin{pmatrix} 0 & \sqrt{M_1^3} & 0 & 0 \\ \sqrt{M_1^3} & M_2^3 & \sqrt{3}M_1 M_2 & \sqrt{3M_1} M_2^2 \\ 0 & \sqrt{3}M_1 M_2 & 0 & \sqrt{M_1^3} \\ 0 & \sqrt{3M_1} M_2^2 & \sqrt{M_1^3} & 2M_1 M_2 \end{pmatrix},$$

where $M_i = M - i$. For example, the entry in the third row, second column of A comes from the $(M-1)^2(M-2)$ type-2 vertices adjacent to a type-3 vertex, times $\sqrt{3(M-1)}$ and divided by $\sqrt{(M-1)^3}$ to convert between the normalizations of $|c\rangle$ and $|b\rangle$. Using this, the search Hamiltonian (3) is

$$H = -\gamma \begin{pmatrix} \frac{1}{\gamma} & \sqrt{M_1^3} & 0 & 0 \\ \sqrt{M_1^3} & M_2^3 & \sqrt{3}M_1 M_2 & \sqrt{3M_1} M_2^2 \\ 0 & \sqrt{3}M_1 M_2 & 0 & \sqrt{M_1^3} \\ 0 & \sqrt{3M_1} M_2^2 & \sqrt{M_1^3} & 2M_1 M_2 \end{pmatrix}.$$

To determine how the search algorithm evolves with this Hamiltonian for large N, we utilize degenerate perturbation theory. In this approach [9,26], we first decompose the Hamiltonian into leading- and higher-order terms:

$$H = H^{(0)} + H^{(1)} + \cdots$$

for large M. From this, we next find the eigenvalues and eigenvectors of $H^{(0)}$, some of which may be degenerate.

Finally, adding the perturbation $H^{(1)}$, certain linear combinations of the degenerate eigenvectors of $H^{(0)}$ are eigenvectors of $H^{(0)} + H^{(1)}$, and this "lifts" the degeneracy. This mixing drives evolution between degenerate eigenvectors of $H^{(0)}$, and the energy or eigenvalue gap dictates the rate of evolution.

We want the perturbation $H^{(1)}$ to mix the marked vertex $|a\rangle$ with the unmarked vertices and drive evolution between them, and this only occurs from the $\langle a|H|b\rangle = \langle b|H|a\rangle = \sqrt{(M-1)^3}$ terms, which is $O(M^{3/2})$, apart from a factor of $-\gamma$. So, $H^{(1)}$ should include terms $\Theta(M^{3/2})$, and $H^{(0)}$ should include anything of higher order, i.e., $\omega(M^{3/2})$:

$$H^{(0)} = -\gamma \begin{pmatrix} \frac{1}{\gamma} & 0 & 0 & 0 \\ 0 & M^3 - 6M^2 & \sqrt{3}M^2 & \sqrt{3}M^{5/2} \\ 0 & \sqrt{3}M^2 & 0 & 0 \\ 0 & \sqrt{3}M^{5/2} & 0 & 2M^2 \end{pmatrix},$$

$$H^{(1)} = -\gamma \begin{pmatrix} 0 & M^{3/2} & 0 & 0 \\ M^{3/2} & 0 & 0 & -\frac{9\sqrt{3}}{2}M^{3/2} \\ 0 & 0 & 0 & M^{3/2} \\ 0 & -\frac{9\sqrt{3}}{2}M^{3/2} & M^{3/2} & 0 \end{pmatrix},$$

$$H^{(2)} = O(\gamma M).$$

With this decomposition, we next need to find the eigenvectors and eigenvalues of $H^{(0)}$, but, unfortunately, this is prohibitively complicated.

To circumvent this obstacle, we can try changing the basis, as in [9,27]. Besides $|a\rangle$, we choose the uniform superposition of unmarked vertices to be another basis state:

$$|r\rangle = \frac{1}{\sqrt{N-1}} \sum_{x \neq w} |x\rangle = \frac{1}{\sqrt{M^3 - 1}} [\sqrt{(M-1)^3}|b\rangle$$
$$+ \sqrt{3(M-1)}|c\rangle + \sqrt{3(M-1)^2}|d\rangle].$$

A state that is obviously orthogonal to this, which we use as a third basis state, is

$$|r'\rangle = \frac{1}{\sqrt{M}}(\sqrt{M-1}|c\rangle - |d\rangle).$$

For the fourth basis state, we take the cross product of $|r\rangle$ and $|r'\rangle$. Abusing notation,

$$|r''\rangle = |r\rangle \times |r'\rangle = \frac{1}{\sqrt{M^3 - 1}} \frac{1}{\sqrt{M}} \begin{vmatrix} |b\rangle & |c\rangle & |d\rangle \\ \sqrt{(M-1)^3} & \sqrt{3(M-1)} & \sqrt{3(M-1)^2} \\ 0 & \sqrt{M-1} & -1 \end{vmatrix}$$

$$= \frac{1}{\sqrt{M^3 - 1}} \frac{1}{\sqrt{M}} [-M\sqrt{3(M-1)}|b\rangle + \sqrt{(M-1)^3}|c\rangle + (M-1)^2|d\rangle].$$

Changing the Hamiltonian from the $\{|a\rangle, |b\rangle, |c\rangle, |d\rangle\}$ basis to the $\{|a\rangle, |r\rangle, |r'\rangle, |r''\rangle\}$ basis, we conjugate it by

$$T = (|a\rangle|r\rangle|r'\rangle|r''\rangle).$$

That is, we calculate $T^{-1}HT$ to get the Hamiltonian in the new basis. Note that in this case, $T^{-1} = T^{\mathsf{T}}$. Doing this and keeping terms at least linear in M, the Hamiltonian in the $\{|a\rangle, |r\rangle, |r'\rangle, |r''\rangle\}$ basis is

$$H' \approx -\gamma \begin{pmatrix} \frac{1}{\gamma} & M^{3/2} & 0 & -\sqrt{3}M \\ M^{3/2} & M^3 - 3M^2 + 3M & 0 & 0 \\ 0 & 0 & 0 & -M^{3/2} \\ -\sqrt{3}M & 0 & -M^{3/2} & -M^2 + 3M \end{pmatrix}.$$

Utilizing degenerate perturbation theory in this new basis, we decompose the Hamiltonian H' into leading- and higher-order matrices:

$$H'^{(0)} = -\gamma \begin{pmatrix} \frac{1}{\gamma} & 0 & 0 & 0 \\ 0 & M^3 - 3M^2 & 0 & 0 \\ 0 & 0 & 0 & 0 \\ 0 & 0 & 0 & -M^2 \end{pmatrix},$$

$$H'^{(1)} = -\gamma \begin{pmatrix} 0 & M^{3/2} & 0 & 0 \\ M^{3/2} & 0 & 0 & 0 \\ 0 & 0 & 0 & -M^{3/2} \\ 0 & 0 & -M^{3/2} & 0 \end{pmatrix}.$$

The eigenvectors and corresponding eigenvalues of $H'^{(0)}$ are now easy to identify, unlike in the old basis. They are

$$|a\rangle, \quad -1,$$
$$|r\rangle, \quad -\gamma(M^3 - 3M^2),$$
$$|r'\rangle, \quad 0,$$
$$|r''\rangle, \quad \gamma M^2.$$

The initial state $|s\rangle$ is approximately $|r\rangle$ for large M, and since we want this to evolve to $|a\rangle$, we make $|a\rangle$ and $|r\rangle$ degenerate by choosing

$$\gamma = \frac{1}{M^2(M-3)}. \tag{4}$$

This is the "critical value" of γ.

Next, we include the perturbation $H'^{(1)}$, which causes linear combinations $\alpha_a|a\rangle + \alpha_r|r\rangle$ to be eigenvectors of $H'^{(0)} + H'^{(1)}$. To find the coefficients, we solve the eigenvalue problem

$$\begin{pmatrix} H_{aa} & H_{ar} \\ H_{ra} & H_{rr} \end{pmatrix} \begin{pmatrix} \alpha_a \\ \alpha_r \end{pmatrix} = E \begin{pmatrix} \alpha_a \\ \alpha_r \end{pmatrix},$$

where $H_{ar} = \langle a|(H'^{(0)} + H'^{(1)})|r\rangle$, etc., and E is the eigenvalue. Evaluating the matrix elements with γ at its critical value (4),

$$\begin{pmatrix} -1 & \frac{-1}{\sqrt{M}(M-3)} \\ \frac{-1}{\sqrt{M}(M-3)} & -1 \end{pmatrix} \begin{pmatrix} \alpha_a \\ \alpha_r \end{pmatrix} = E \begin{pmatrix} \alpha_a \\ \alpha_r \end{pmatrix}.$$

Solving this, we get the following eigenvectors and eigenvalues of $H'^{(0)} + H'^{(1)}$:

$$\begin{pmatrix} \alpha_a \\ \alpha_r \end{pmatrix} = \frac{1}{\sqrt{2}} \begin{pmatrix} 1 \\ 1 \end{pmatrix}, \quad E_0 = -1 - \frac{1}{\sqrt{M}(M-3)},$$

$$\begin{pmatrix} \alpha_a \\ \alpha_r \end{pmatrix} = \frac{1}{\sqrt{2}} \begin{pmatrix} -1 \\ 1 \end{pmatrix}, \quad E_1 = -1 + \frac{1}{\sqrt{M}(M-3)}.$$

Since the eigenvectors are proportional to $\pm|a\rangle + |r\rangle$, the system evolves from $|s\rangle \approx |r\rangle$ to $|a\rangle$, up to a phase, in time

$$\frac{\pi}{\Delta E} = \frac{\pi}{2}\sqrt{M}(M-3) \approx \frac{\pi}{2} M^{3/2} \approx \frac{\pi}{2}\sqrt{N},$$

where $\Delta E = E_1 - E_0$ is the energy gap. This is the same runtime as the first-order Kronecker graph (i.e., complete graph) and second-order Kronecker graph. A simulation is shown in Fig. 7, and the success probability reaches 1 at time $\pi\sqrt{256^3}/2 \approx 6433.98$, as expected.

These results are asymptotic, meaning M must be sufficiently large in order for the success probability to reach 1 at time $\pi\sqrt{N}/2$. Numerically, choosing γ to be $1/(M-1)^3$, rather than $1/M^2(M-3)$ that we derived earlier, allows smaller values of M to exhibit this asymptotic runtime. Taylor expanding the two values of γ for large M,

$$\frac{1}{(M-1)^3} = \frac{1}{M^3} + \frac{3}{M^4} + \frac{6}{M^5} + O\left(\frac{1}{M^6}\right),$$

$$\frac{1}{M^2(M-3)} = \frac{1}{M^3} + \frac{3}{M^4} + \frac{9}{M^5} + O\left(\frac{1}{M^6}\right).$$

Thus, the two values of γ are equal, up to terms of order $1/M^5$.

V. HIGHER ORDERS

In theory, we can apply the same perturbative approach from the third-order case to Kronecker graphs with order $j \geqslant 4$. Analyzing an infinite number of these cases in this iterative manner, however, is prohibitive due to the countably infinite possible values for j. Further complicating the matter is that the dimension of the subspace increases with j, so perturbation theory would be used to find the eigenvalues and eigenvectors of progressively larger matrices, making generalization of our results difficult. For example, when $j = 1$, the complete graph
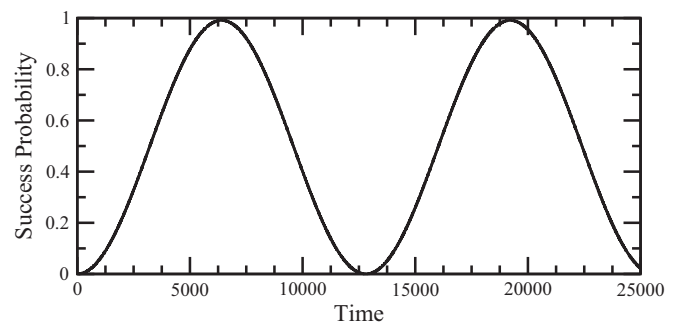

FIG. 7. Success probability as a function of time for search by continuous-time quantum walk on $K_M \otimes K_M \otimes K_M$ with $M = 256$.
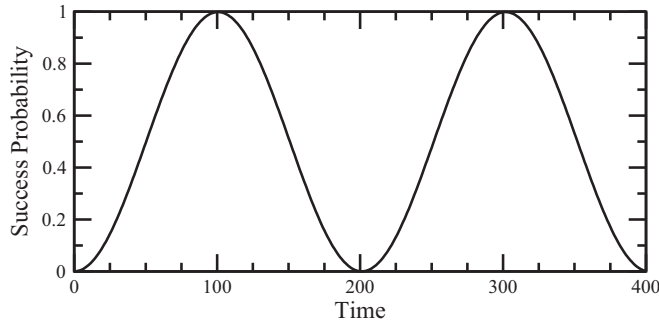
FIG. 8. Success probability as a function of time for search by continuous-time quantum walk on the sixth-order Kronecker graph $K_M \otimes K_M \otimes K_M \otimes K_M \otimes K_M \otimes K_M$ with $M = 4$ and $\gamma = 0.001372$.

evolves in a 2D subspace, when $j = 2$, the strongly regular graph evolves in a 3D subspace, and when $j = 3$, the graph evolves in a 4D subspace.

Numerical simulations do suggest, however, that search on higher-order Kronecker graphs with the complete initiator also takes $\pi\sqrt{N}/2$ time, asymptotically. For example, the success probability for search on a sixth-order Kronecker graph is shown in Fig. 8, and it reaches 1 at time $\pi\sqrt{4^6}/2 \approx 100.53$. Similarly, numerical simulations show that increasing j and keeping M fixed, or increasing both j and M, yields a successful search in $\pi\sqrt{M^j}/2$ time.

Despite the increase in the dimension of the subspace, we can prove that the diameter of the Kronecker graph, with complete initiator, is 2 for all $j \geqslant 2$ and $M \geqslant 3$. To do this, note a general vertex $|v\rangle$ can be written as

$$|v\rangle = |p_1, p_2, \ldots, p_j\rangle,$$

where each p_i takes values $1, \ldots, M$ and encodes the position at each level of hierarchy. For example, in Fig. 8, if $p_i = 1$ encodes the top-left position, then vertex 1 would be $|1, 1, 1\rangle$ since it is the top-left vertex in its subset $P_{1,1}$, its subset $P_{1,1}$ is the top-left subset in its set P_1, and P_1 is the top-left set. A vertex nonadjacent to $|v\rangle$ has the general form

$$|u\rangle = |p_1', p_2', \ldots, p_j'\rangle,$$

where at least one $p_i' = p_i$ since, if all of the positions were to differ, the vertices would be adjacent. Now consider a third vertex,

$$|w\rangle = |p_1'', p_2'', \ldots, p_j''\rangle,$$

where $p_i'' \neq p_i$ and $p_i'' \neq p_i'$. This is possible since $M \geqslant 3$. Then, $|w\rangle$ is adjacent to both $|v\rangle$ and $|u\rangle$, so the distance between $|v\rangle$ and $|u\rangle$ is 2, and the diameter of the graph is 2.

VI. CONCLUSION

Kronecker graphs are a useful method to generate complex networks with real-world properties. Here, we investigated how continuous-time quantum walks search Kronecker graphs by focusing on the case that the initiator is the complete graph. Then, the first-order Kronecker graph is exactly the quantum

walk formulation of Grover's algorithm, where the search takes $\pi\sqrt{N}/2$ time. We proved that second-order Kronecker graph is a strongly regular graph, and that it is also searched in $\pi\sqrt{N}/2$ time. Furthermore, using degenerate perturbation theory, we proved that the third-order Kronecker graph is searched in the same optimal runtime as the first- and second-order graphs. Numerical simulations indicate that higher-order Kronecker graphs behave the same way, and an analytical proof is open for further research. Our work on quantum search on Kronecker graphs, where the initiator is not the complete graph, will be reported elsewhere.

APPENDIX: 4D SUBSPACE FOR THIRD-ORDER KRONECKER GRAPHS

Recall for the third-order Kronecker graph with complete initiator that there are four types of vertices. Let us begin by determining how many of each type of vertex there is using the $M = 4$ case in Fig. 6 and then generalizing to arbitrary M.

The first type of vertex is the unique marked vertex, say vertex 1, so there is only one vertex of the first type. Next, we count the number of vertices adjacent to vertex 1, which are the vertices in a different set, different subset, and different position within the subset from the marked vertex. Vertex 1 has adjacent vertices in $(4 - 1) = 3$ sets, namely, in P_2, P_3, and P_4. Within each of these sets, vertex 1 has adjacent vertices in $(4 - 1) = 3$ of the subsets, such as $P_{2,2}$, $P_{2,3}$, and $P_{2,4}$. Within a subset, vertex 1 is adjacent to $(4 - 1) = 3$ vertices, such as vertices 22, 23, and 24. So vertex 1 has $(4 - 1)^3 = 27$ neighbors. Generalizing this, there are $(M - 1)^3$ vertices adjacent to the marked vertex, and these are vertices of the second type.

The third and fourth types of vertices are nonadjacent to the marked vertex. Let us tabulate the vertices that are nonadjacent to the marked vertex, showing that they either share $(M - 1)^2(M - 2)$ mutual neighbors with the marked vertex or $(M - 1)(M - 2)^2$ mutual neighbors with the marked vertex.

Vertices that are in the same subset as the marked vertex are nonadjacent to the marked vertex. For example, in Fig. 6, if vertex 1 is marked, then vertices 2, 3, and 4 are in the same subset as vertex 1 and are nonadjacent to vertex 1. In general, there are $(M - 1)$ such vertices. Let us take vertex 2, for example. Vertices 1 and 2 share no common neighbors in P_1 since they are nonadjacent to all vertices in P_1. Within each of the $(4 - 1) = 3$ remaining sets P_2, P_3, and P_4, they share adjacent vertices in $(4 - 1) = 3$ subsets, such as $P_{2,2}$, $P_{2,3}$, and

TABLE I. For the third-order Kronecker graph $K_M \otimes K_M \otimes K_M$, the types of vertices that are nonadjacent to the marked vertex, how many such vertices there are, and the number of mutual neighbors each vertex has with the marked vertex.

Description of nonadjacent vertex	Number of vertices	Number of mutual neighbors
Same set, same subset, different position	$M-1$	$(M-1)^2(M-2)$
Same set, different subset, same position	$M-1$	$(M-1)^2(M-2)$
Same set, different subset, different position	$(M-1)^2$	$(M-1)(M-2)^2$
Different set, same subset, same position	$M-1$	$(M-1)^2(M-2)$
Different set, same subset, different position	$(M-1)^2$	$(M-1)(M-2)^2$
Different set, different subset, same position	$(M-1)^2$	$(M-1)(M-2)^2$

$P_{2,4}$ in P_2. Within each subset, there are $(4-2) = 2$ mutually adjacent vertices, such as vertices 23 and 24 in $P_{2,2}$. So, the total number of common neighbors is $(4-1)(4-1)(4-2) = 18$. Generalizing this, there are $(M-1)(M-1)(M-2) = (M-1)^2(M-2)$ mutual neighbors. This is summarized in the first row of Table I.

A vertex that is nonadjacent to the marked vertex could be in the same set as the marked vertex, but a different subset, yet in the same position within its subset as the marked vertex is within its subset. In Fig. 6, these vertices would be vertices 5, 9, and 13. In general, there are $(M-1)$ such nonadjacent vertices. Let us take vertex 5, for example. Vertices 1 and 5 share no common neighbors in P_1, so $(4-1) = 3$ sets remain where they can have common neighbors. Within these sets, say P_2, there are no common neighbors in the top two subsets $P_{2,1}$ or $P_{2,2}$. This leaves $(4-2) = 2$ subsets $P_{2,3}$ and $P_{2,4}$ that contain mutual neighbors, and within each of these subsets, such as $P_{2,3}$, there are $(4-1) = 3$ mutual neighbors. So the total number of common neighbors is $(4-1)(4-2)(4-1) = 18$, as in the previous case, or $(M-1)(M-2)(M-1) = (M-1)^2(M-2)$ in general. This is summarized in the second row of Table I.

Another vertex that is nonadjacent to the marked vertex is one in the same set as the marked vertex, but a different subset, and in a different position. In Fig. 6, these are vertices 6, 7, 8, 10, 11, 12, 14, 15, and 16, and, in general, there are $(M-1)^2$ such vertices. Let us take vertex 6, for example. Vertices 1 and 6 have mutual neighbors in the three remaining sets P_2, P_3, and P_4. In general, there are $(M-1)$ such sets. With a set, say P_2, there are $(4-2) = 2$ subsets $P_{2,3}$ and $P_{2,4}$ that contain mutual neighbors of vertices 1 and 6. In general, there are $(M-2)$ such subsets within each set. Finally, within each subset, say within $P_{2,3}$, vertices 27 and 28 are mutual neighbors of vertices 1 and 6, and, in general, there are $(M-2)$ mutual neighbors in each subset. Altogether, there are $(M-1)(M-2)(M-2) = (M-1)(M-2)^2$ mutual neighbors. This is summarized in the third row of Table I.

A vertex in a different set from the marked vertex, but in the same position, is also nonadjacent to the marked vertex. In Fig. 6, these vertices would be vertices 17, 33, and 49, and, in general, there are $(M-1)$ such vertices. How many

mutual neighbors does one of these vertices have with the marked vertex? There are $(M-2)$ sets that contain mutual neighbors, each with $(M-1)$ subsets that contain mutual neighbors, each with $(M-1)$ mutually adjacent vertices, for a total of $(M-2)(M-1)(M-1) = (M-1)^2(M-2)$ mutual neighbors. This is summarized in the fourth row of Table I.

One more kind of vertex that is nonadjacent to the marked vertex is one in a different set from the marked vertex, the same relative subset, but a different position within the subset. In Fig. 6, this corresponds to vertices 18, 19, 20, 34, 35, 36, 50, 51, and 52. In general, there are $(M-1)^2$ such vertices. Taking one of these vertices and the marked vertex 1, there are $(M-2)$ sets containing mutual neighbors, each with $(M-1)$ subsets containing mutual neighbors, each with $(M-2)$ mutual neighbors, for a total of $(M-1)(M-2)^2$ mutual neighbors. This is summarized in the fifth row of Table I.

Finally, the last kind of vertex that is nonadjacent to the marked vertex lies in a different set, in a different relative subset, but the same position within the subset as the marked vertex. In Fig. 6, this corresponds to vertices 21, 25, 29, 37, 41, 45, 53, 57, and 61. In general, there are $(M-1)^2$ such vertices. Taking one of these vertices and the marked vertex 1, there are $(M-2)$ sets containing mutual neighbors, each with $(M-2)$ subsets containing mutual neighbors, each with $(M-1)$ mutual neighbors, for a total of $(M-1)(M-2)^2$ mutual neighbors. This is summarized in the last row of Table I.

Summarizing these results, in total, there are $3(M-1)$ vertices that are nonadjacent to the marked vertex, each with $(M-1)^2(M-2)$ mutual neighbors with the marked vertex. Also, in total, there are $3(M-1)^2$ vertices that are nonadjacent to the marked vertex, each with $(M-1)(M-2)^2$ mutual neighbors with the marked vertex. This divides the vertices that are nonadjacent to the marked vertex into type-3 and type-4 vertices.

Lastly, as a sanity check, we add the one marked vertex, the number of adjacent vertices, and the number of nonadjacent vertices of each type:

$$1 + (M-1)^3 + 3(M-1) + 3(M-1)^2 = M^3 = N.$$

We get the total number of vertices, as expected.

[1] L. K. Grover, A fast quantum mechanical algorithm for database search, in *Proceedings of the 28th Annual ACM Symposium on Theory of Computing, STOC 1996* (ACM Press, New York, 1996), pp. 212–219.

[2] M. A. Nielsen and I. L. Chuang, *Quantum Computation and Quantum Information* (Cambridge University Press, Cambridge, 2000).

[3] P. Benioff, Space searches with a quantum robot, in *Quantum Computation and Information*, Contemp. Math. (Amer. Math. Soc., Providence, RI, 2002), Vol. 305, pp. 1–12.

[4] D. A. Meyer, From quantum cellular automata to quantum lattice gases, J. Stat. Phys. **85**, 551 (1996).

[5] D. A. Meyer, On the absence of homogeneous scalar unitary cellular automata, Phys. Lett. A **223**, 337 (1996).

[6] S. Aaronson and A. Ambainis, Quantum search of spatial regions, Theor. Comput. **1**, 47 (2005).

[7] A. M. Childs and J. Goldstone, Spatial search by quantum walk, Phys. Rev. A **70**, 022314 (2004).

[8] A. Ambainis, J. Kempe, and A. Rivosh, Coins make quantum walks faster, in *Proceedings of the 16th Annual ACM-SIAM Symposium on Discrete Algorithms, SODA 2005* (SIAM, Philadelphia, PA, 2005), pp. 1099–1108.

[9] J. Janmark, D. A. Meyer, and T. G. Wong, Global Symmetry is Unnecessary for Fast Quantum Search, Phys. Rev. Lett. **112**, 210502 (2014).

[10] D. A. Meyer and T. G. Wong, Connectivity is a Poor Indicator of Fast Quantum Search, Phys. Rev. Lett. **114**, 110503 (2015).

[11] S. Chakraborty, L. Novo, A. Ambainis, and Y. Omar, Spatial Search by Quantum Walk is Optimal for Almost all Graphs, Phys. Rev. Lett. **116**, 100501 (2016).

[12] J. Kempe, Quantum random walks: An introductory overview, Contemp. Phys. **44**, 307 (2003).

[13] S. Milgram, The small-world problem, Psychol. Today **1**(1), 61 (1967).

[14] A.-L. Barabási and R. Albert, Emergence of scaling in random networks, Science **286**, 509 (1999).

[15] J. Leskovec and A. Krevl, SNAP Datasets: Stanford large network dataset collection, http://snap.stanford.edu/data (unpublished).

[16] M. P. H. Stumpf, C. Wiuf, and R. M. May, Subnets of scale-free networks are not scale-free: Sampling properties of networks, Proc. Natl. Acad. Sci. USA **102**, 4221 (2005).

[17] J. Leskovec, J. Kleinberg, and C. Faloutsos, Graphs over time: Densification laws, shrinking diameters and possible explanations, in *Proceedings of the 11th ACM SIGKDD International Conference on Knowledge Discovery in Data Mining, KDD 2005* (ACM Press, New York, 2005), p. 177.

[18] J. Leskovec, D. Chakrabarti, J. Kleinberg, and C. Faloutsos, Realistic, mathematically tractable graph generation and evolution, using Kronecker multiplication, in *Proceedings of the 9th European Conference on Principles and Practice of Knowledge Discovery in Databases, PKDD 2005* (Springer, Berlin, 2005), p. 133.

[19] J. Leskovec and C. Faloutsos, Scalable modeling of real graphs using Kronecker multiplication, in *Proceedings of the 24th International Conference on Machine Learning, ICML 2007* (ACM Press, New York, 2007), p. 497.

[20] J. Leskovec, D. Chakrabarti, J. Kleinberg, C. Faloutsos, and Z. Ghahramani, Kronecker graphs: An approach to modeling networks, J. Mach. Learn. Res. **11**, 985 (2010).

[21] G. Brassard, P. Høyer, M. Mosca, and A. Tapp, Quantum amplitude amplification and estimation, in *Quantum Computation and Information*, Contemp. Math. (Amer. Math. Soc., Providence, RI, 2002), Vol. 305, p. 53.

[22] E. Farhi and S. Gutmann, Analog analogue of a digital quantum computation, Phys. Rev. A **57**, 2403 (1998).

[23] T. G. Wong, Grover search with lackadaisical quantum walks, J. Phys. A: Math. Theor. **48**, 435304 (2015).

[24] C. Godsil (private communication).

[25] P. J. Cameron and J. H. van Lint, *Designs, Graphs, Codes and Their Links*, London Mathematical Society Student Texts (Cambridge University Press, Cambridge, 1991).

[26] T. G. Wong, Diagrammatic approach to quantum search, Quantum Inf. Process. **14**, 1767 (2015).

[27] T. G. Wong, Quantum walk search on Johnson graphs, J. Phys. A: Math. Theor. **49**, 195303 (2016).